Ultrafast, solid-state oscillators based on broadband, multisite Yb-doped crystals

Federico Pirzio,[1,*] Matthias Kemnitzer,[2] Annalisa Guandalini,[2] Florian Kienle,[2] Stefano Veronesi,[3] Mauro Tonelli,[3] Juerg Aus der Au,[2] and Antonio Agnesi[1]

[1]*Università di Pavia, Dipartimento di Ingegneria Industriale e dell' Informazione, Via Ferrata 5, 27100 Pavia, Italy*

[2]*Spectra-Physics Rankweil, Feldgut 9, Rankweil A-6830, Austria*

[3]*NEST Istituto Nanoscienze-CNR and Dipartimento di Fisica, Università di Pisa, Largo B. Pontecorvo 3, IT-56127 Pisa, Italy*

[*]*federico.pirzio@unipv.it*

Abstract: A detailed performance comparison of new interesting Yb-doped crystals in the same oscillator setup, with a single-mode fiber-coupled diode laser pump, is reported. We intended to assess the shortest pulses achievable with available SESAM technology, running a fair comparison with laser crystals Yb:KLuW, Yb:SSO, Yb:CALGO, Yb:CALYO and Yb:CaF_2, very likely including the most promising choices for the next generation of commercial bulk ultrafast solid-state systems.

OCIS codes: (140.3615) Lasers, ytterbium; (140.7090) Ultrafast lasers.

References and links

1. K. C. Phillips, H. H. Gandhi, E. Mazur, and S. K. Sundaram, "Ultrafast laser processing of materials: a review," Adv. Opt. Photon. **7**, 684–712 (2015).
2. K. Sugioka, and Y. Cheng, "Ultrafast lasers – reliable tools for advanced materials processing," Light Sci Appl. **3**, e149 (2014).
3. W. Sibbett, A. A. Lagatsky, and C. T. A. Brown, "The development and application of femtosecond laser systems," Opt. Express **20**, 6989–7001 (2012).
4. N. V. Kuleshov, A. A. Lagatsky, A. V. Podlipensky, and V. P. Mikhailov, and G. Huber, "Pulsed laser operation of Yb-doped $KY(WO_4)_2$ and $KGd(WO_4)_2$," Opt. Lett. . **22**, 1317–1319 (1997).
5. F. Brunner, G. J. Spühler, J. Aus der Au, L. Krainer, F. Morier-Genoud, R. Paschotta, N. Lichtenstein, S. Weiss, C. Harder, A. A. Lagatsky, A. Abdolvand, N. V. Kuleshov, and U.Keller, "Diode-pumped femtosecond Yb:$KGd(WO_4)_2$ laser with 1.1-W average power, Opt. Lett. **25**, 1119–1121 (2000).
6. V. Petrov, M. C. Pujol, X. Mateos, O. Silvestre, S. Rivier, M. Aguiló, R. M. Solé, J. Liu, U.Griebner, and F. Diaz, "Growth and properties of $KLu(WO_4)_2$, and novel Ytterbium and Thulium lasers based on this monoclinic crystalline host," Laser & Photon. Rev. **1**, 179–212 (2007).
7. L. Zheng, J. Xu, G. Zhao, L. Su, F. Wu, and X. Liang, "Bulk crystal growth and efficient diode-pumped laser performance of Yb^{3+}:Sc_2SiO_5, Appl. Phys. B **91**, 443–445 (2008).
8. F. Druon, S. Ricaud, D. Papadopoulos, A. Pellegrina, P. Camy, J. Doualan, R. Moncorgé, A. Courjaud, E. Mottay, and P. Georges, "On Yb:CaF_2 and Yb:SrF_2: review of spectroscopic and thermal properties and their impact on femtosecond and high power laser performance," Opt. Mater. Express **1**, 489–502 (2011).
9. E. Caracciolo, M. Kemnitzer, A. Guandalini, F. Pirzio, A. Agnesi, and J. Aus der Au, "High pulse energy multi-watt Yb:$CaAlGdO_4$ and Yb:CaF_2 regenerative amplifiers," Opt. Express **22**, 19912–19918 (2014).
10. F. Pirzio, S. Cafiso, M. Kemnitzer, A. Guandalini, F. Kienle, S. Veronesi, M. Tonelli, J. Aus der Au, and A. Agnesi, "Sub-50-fs widely tunable Yb:$CaYAlO_4$ laser pumped by 400-mW single-mode fiber-coupled laser diode," Opt. Express **23**, 9790–9795 (2015).
11. F. Pirzio, E. Caracciolo, M. Kemnitzer, A. Guandalini, F. Kienle, J. Aus der Au, and A. Agnesi, "Performance of Yb:Sc_2SiO_5 crystal in diode-pumped femtosecond oscillator and regenerative amplifier," Opt. Express **23**, 13115–13120 (2015).

#262554 Received 5 Apr 2016; revised 11 May 2016; accepted 11 May 2016; published 20 May 2016

12. E. Caracciolo, M. Kemnitzer, A. Guandalini, F. Pirzio, J. Aus der Au, and A. Agnesi, "28-W, 217 fs solid-state Yb:$CaGdAlO_4$ regenerative amplifiers, Opt. Lett. **38**, 4131–4133 (2013).
13. A. Greborio, A. Guandalini, J. Aus Der Au, "Sub-100 fs pulses with 12.5 W from Yb:CALGO based oscillator," Proc. SPIE, **8235** (2012).
14. F. Pirzio, S. Di Dio Cafiso, M. Kemnitzer, F. Kienle, A. Guandalini, J. Aus der Au, and A. Agnesi, "65-fs Yb:CaF_2 laser mode-locked by semiconductor saturable absorber mirror," J. Opt. Soc. Am. B **32**, 2321–2325 (2015).
15. J. A. Caird, S. A. Payne, P. R. Staber, A. J. Ramponi, L. L. Chase, and W. F. Krupke, "Quantum electronic properties of the $Na_3Ga_2Li_3F_{12}$:Cr^{3+} laser, IEEE J. Quantum Electron. **24**, 1077–1099 (1988).
16. D. Kopf, G. J. Spühler, K. J. Weingarten, and U. Keller, "Mode-locked laser cavities with a single prism for dispersion compensation, Appl. Opt. **35**, 912–915 (1996).
17. A. Agnesi, A. Greborio, F. Pirzio, E. Ugolotti, G. Reali, A. Guandalini, and J. Aus der Au, "Diode-pumped passively mode-locked tunable Yb:CALGO solid-state laser, J. Opt. Soc. Am. B **30**, 1513–1516 (2013).
18. C. Hönninger, R. Paschotta, F. Morier-Genoud, M. Moser, and U. Keller, "Q-switching stability limits of continuous-wave passive mode locking, J. Opt. Soc. Am. B **16**, 45–56 (1999).
19. P. Sévillano, P. Georges, F. Druon, D. Descamps, and E. Cormier, "32-fs Kerr-lens mode-locked Yb:$CaGdAlO_4$ oscillator optically pumped by a bright fiber laser," Opt. Lett. **39**, 6001–6004 (2014).

1. Introduction

High-power multiwatt solid-state lasers near 1 μm wavelength have become successful tools in many industrial and medical applications [1–3]. The first generation of such lasers was based on the best materials investigated to this aim in the late 1990s, i.e. Yb-doped tungstates such as Yb:KYW and Yb:KGW [4, 5]. Wide-bandwidth laser crystals with reasonably good thermo-mechanical features, together with the fast-developing high-power laser diode technology for pumping near 980 nm have been the key elements for the success of this ultrafast laser platform in the demanding industrial world. However, the quest for superior performance in terms of shorter pulses and higher power has pushed the material research to the point that new extremely promising materials are now being incorporated in the next generation of ultrafast solid-state lasers. This article reports our comparative investigation of what we consider the most promising multisite broadband Yb-doped crystals for the next commercial products, from the point of view of the bulk oscillators. In particular:

- Yb:KLuW is the next step for tungstate technology, owing to the favorable matching of Yb^{3+} and Lu^{3+} ion size that reduces the impact of dopant concentration on thermal and mechanical crystal properties [6].
- Yb:SSO is the most promising candidate belonging to the family of silicates, with thermal conductivity $\approx$ 70% that of Yb:YAG, much wider fluorescence bandwidth of $\approx$ 50 nm and transparency pump intensity as small as 2% of Yb:YAG [7].
- Yb:CaF_2 is the most promising fluoride crystal, possessing a broad emission band of $\approx$ 70 nm, though not exceptional for thermal management [8, 9].
- Yb:CALGO and Yb:CALYO are extremely interesting for comparable broad emission bandwidth and very good thermal properties [9, 10].

We already reported extensive investigations on regenerative amplifiers based on Yb:SSO [11], Yb:CaF_2 [9], and Yb:CALGO [9, 12]. The scope of this work was to assess the best performance of the oscillators based on all these crystals, in terms of pulse duration, with state-of-the-art SESAM mode-locking. Since Yb-doped materials are relatively broadband, but with mode-locking tunability limited to few tens nm, or even less in some cases, in many practical situations it is preferable to use the same laser material in the seeder and in the regenerative amplifier, for better matching of the central wavelength.

#262554 Received 5 Apr 2016; revised 11 May 2016; accepted 11 May 2016; published 20 May 2016

Furthermore, we believe that the most accurate and effective comparison of this set of laser crystals can be done only with the same setup in terms of pump laser and resonator configuration. Of course, optimization of each particular oscillator requires slight modifications in terms of dispersion management and focusing on the SESAM.

As for the pump device we chose low-power 400-mW fiber-coupled single-mode laser diodes, wavelength stabilized with a fiber Bragg grating (FBG). This allows straightforward mode-matching and gain optimization in all crystals investigated, with no additional thermal issues that would complicate the interpretation of the results.

Higher power oscillator can be designed as already reported [13,14], but these require careful consideration of the markedly different thermal properties of the crystals investigated, generally trading off pulse width and output power. Furthermore, for seeding regenerative amplifiers a relatively modest power level is sufficient, which is also true for imaging applications.

2. Experiments

The list of the active materials we investigated in our experiments with their length, dopant concentration and the more relevant spectroscopic and thermo-optical properties is reported in Table 1.

Table 1. List of the active media we tested with the corresponding length and dopant concentration and more relevant spectroscopic and thermo-optical properties.

Reference	Yb:KLuW [6]	Yb:SSO [7]	Yb:CALGO [9]	Yb:CALYO [10]	Yb:CaF_2 [8]
Doping [%at.]	5%	5%	2%	5%	5%
Yb^{3+} dens. [10^{20} cm^{-3}]	4.3	10.6	2.5	6.25	12.25
Length [mm]	2	2.91	4	2	3
λ_p [nm]	981	976	979	979	980
peak σ_a [10^{-20} cm^2]	11.8$\|\|$ N_m	10.9	3.4$\|\|$ c	4.4$\|\|$ c	0.54
$\Delta\lambda_p$ FWHM [nm]	3.6$\|\|$ N_m	24	5	8	8
peak σ_e [10^{-20} cm^2]	1.24$\|\|$ N_p	0.44	0.75$\|\|$ a	0.75$\|\|$ a	0.17
$\Delta\lambda_g$ FWHM [nm]	$\sim$ 28	$\sim$ 20	$\sim$ 80	$\sim$ 80	$\sim$ 70
τ_f [ms]	0.3	1.64	0.45	0.45	2.4
n	1.99$\|\|N_p$, 2.03$\|\|N_m$	1.85	1.84	1.84	1.43
n_2 [m^2W^{-1}]	n.a.	n.a.	9	n.a.	2.5
k [$Wm^{-1}K^{-1}$]	2.55$\|\|$ N_p, 3.09$\|\|N_m$	7.5	6.9$\|\|$ a	3.6$\|\|$ a	6
$\frac{dn}{dT}$ [$10^{-6}K^{-1}$]	n.a.	-6.3	n.a.	n.a.	-10.6

In order to better compare their performance, we tested all the samples in the same laser setup. As it is shown in Fig. 1, the pump system consisted of a 400-mW, single-mode fiber-coupled (FC) laser diode (JDSU S27-7602-400) emitting at 976 nm. The laser diode output beam was not polarized, but by properly coiling the fiber pig-tail we were able to induce a strongly elliptical polarization with a ratio of about 13:1 between the two axes. Given the transmission of the optical elements in the pump path, the maximum incident pump power was about 370 mW. A half-wave plate (HWP) was used to adjust the principal axis along the proper direction to optimize the pump absorption in each material. In case of Yb:SSO experiments, despite

#262554 Received 5 Apr 2016; revised 11 May 2016; accepted 11 May 2016; published 20 May 2016

the monoclinic crystal structure [7], we did not observe any significant dependence of the pump absorption on the pump beam polarization.

In case of Yb:CaF_2 experiments, given the lower value of absorption cross section with respect to all the other available materials, we modified the pump module adding a second single-mode fiber-coupled laser diode, identical to the first one. In this case, we combined the two pump beams through a polarizer and spatially overlapped them before focussing in the active medium. In this configuration, the maximum incident pump power was about 640 mW equally distributed between the two polarizations. The pump beam telescope (see Fig. 1) consisted of an aspherical collimating lens L1 and a spherical focussing lens L2 yielding a pump beam waist radius of w = 12 μm in the active medium. It is worth noticing that owing to the perfectly circular shape and close-to-ideal TEM_{00} beam profile, this pump system yields the highest gain per Watt of absorbed power, and the lowest thermal stress in the crystal. This is a clear advantage with respect to multiwatt, multimode diode pumping, since it helps optimize the mode-matching and minimizes the thermal lensing effects, resulting in lower thresholds, higher efficiency and an easier optimization of the oscillator for minimum pulse duration in mode-locked (ML) regime.

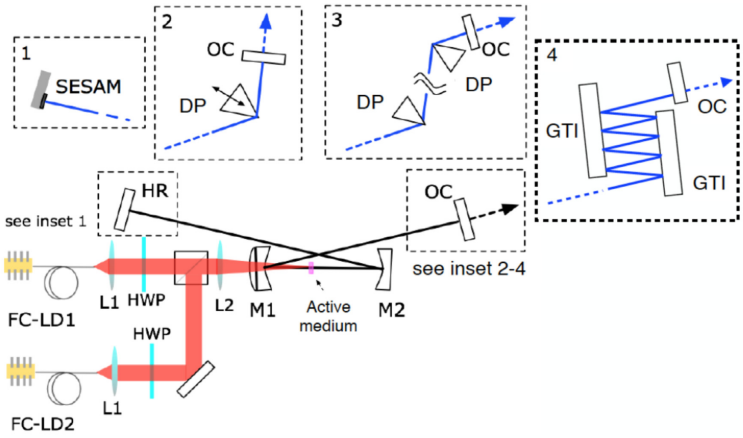

Fig. 1. Setup for the CW laser and (inset) ML experiments. FC-LD: Single-mode fiber-coupled laser diode; L1: Aspherical lens (f = 15.3 mm, NA 0.16); HWP: Half-wave plate AR coated at 976 nm; L2: Spherical lens (50 mm focal); M1: Concave mirror, R = 50 mm, high reflectivity (HR) at 1000-1100 nm, high transmissivity at 940-980 nm; M2: Concave mirror, 100 mm radius of curvature; HR: Flat mirror HR between 1000 and 1100 nm; OC: Output coupler, 30' wedge; DP: Dispersive prisms; GTI: Gires-Tournois Interferometric mirrors, HR at 1000-1100 nm, -55 fs^2 per bounce; SESAM: Semiconductor saturable absorber mirror. The second FC-LD was only used for the Yb:CaF_2 experiments.

The X-folded resonator layout for continuous wave (CW) and ML operations is shown in Fig. 1. All the samples were antireflection (AR) coated at both the pump and laser wavelengths and were simply placed on a metallic plate and oriented with a small tilt angle with respect to the normal incidence direction in order to avoid unwanted etalon effects and back reflections toward the pump. In order to minimize the cavity mode astigmatism in the active media, the resonator curved mirror folding angles were kept as small as possible. Given the mechanical constraints, this corresponded to an angle of incidence on M1, M2 of about 2.2°. In both CW and ML operation, we exploited the resonator stability region corresponding to a larger separation M1-M2. Therefore, we could control the cavity mode waist on the HR mirror by properly adjusting the distance M2-HR and M1-M2 separation.

#262554 Received 5 Apr 2016; revised 11 May 2016; accepted 11 May 2016; published 20 May 2016

Table 2. Summary of the CW regime results.

	Yb:KLuW	Yb:SSO	Yb:CALGO	Yb:CALYO	Yb:CaF_2
P_{ab}^{max} [mW]	320	346	310	350	440
P_{out}^{max} [mW]	211	233	154	155	242
P_{ab}^{th} [mW] (T_{oc}=0.8%)	18	25	40	45	27
T_{oc}^{opt}	5%	5%	2.5%	5%	5%
Max CW slope eff.	76%	72%	50%	45%	55%
η_0	0.85	0.8	0.74	0.7	0.83
δ_c	0.6%	0.3%	0.7%	1.1%	1.5%

Through ABCD modeling of the resonator, we could estimate a fundamental cavity mode dimension in the active medium ranging from 12 to 15 μm within the stability region depending on the total resonator length.

2.1. Continuous-wave experiments results

At first we tested all the samples in CW regime. During these experiments, the mirrors distances were the following: M1-M2: 94 mm; M2-HR: 200 mm; M1-OC: 400 mm. The results obtained with the different materials are summarized in Table 2.

The maximum absorbed pump power P_{ab}^{max} was similar for all the materials (only slightly higher in case of Yb:CaF_2 due to the doubling of the incident pump power) and laser thresholds P_{ab}^{th} of few tens of mW with T = 0.8% output coupler (OC) were measured in all the experiments. In order to assess the total (cavity + crystal) losses δ_c, and the intrinsic slope efficiency η_0, we performed a Caird slope analysis fitting the measured slope efficiency as a function of the output coupling with the following equation [15]:

$$\eta = \eta_0 \frac{\lambda_p}{\lambda_l} \frac{-\ln(R_{oc})}{\delta_c - \ln(R_{oc})} \tag{1}$$

where λ_p and λ_l are the pump and laser output wavelength, respectively. Although the laser output wavelength depends on the output coupler reflectivity for all broadband, quasi-three-level Yb-doped materials, in our experiments the highest variability in output wavelength was observed for Yb:CALYO and Yb:CALGO. For these two materials, the laser output wavelength in CW regime moved from 1060 to 1045 nm for the OC transmission varying from 0.8% to 10%. This corresponds to a maximum modification of the λ_p/λ_l factor in Eq. (1) of only 1.4%. Thus, the ratio λ_p/λ_l in Eq. (1) can be considered reasonably constant. Moreover, please note that δ_c does not include reabsorption losses, which contribute to the laser threshold, but do not affect the laser performance above the threshold, when they are saturated by the intense intracavity laser field. The intrinsic slope efficiency η_0 in Eq. (1) takes into account parameters such as the laser crystal quantum efficiency and mode-matching efficiency. The high values of η_0 obtained ($\eta_0 \geq 0.7$ for each material we tested, see Table 2) suggest a well optimized resonator design. The differences in resonator intrinsic losses estimated through the Caird analysis can be mainly attributed to different optical quality of the AR coating of the crystal facets or to slightly different residual scattering losses in the disordered crystals, since the resonator mirrors we employed were the same in all the experiments.

#262554 Received 5 Apr 2016; revised 11 May 2016; accepted 11 May 2016; published 20 May 2016

2.2. *Mode-locking regime*

For the ML experiments, we modified the resonator as depicted in Fig. 1. The high-reflectivity (HR) flat mirror was replaced by a 3% modulation loss, 140 μJ/cm^2 saturation fluence SESAM provided by Spectra-Physics Rankweil. For intracavity Group Delay Dispersion (GDD) management, we tested different configurations depending on the active material employed and on the main goal of the experiment. When the minimum attainable pulse duration was the main concern, we opted for a cavity configuration employing a pair of dispersive prisms (DPs) (see inset 3 of figure 1). If compared to Gires-Tournois Interferometric mirrors (GTI), DPs offers significant advantages, namely the amount of dispersion can be continuously varied and the dispersion introduced is almost constant over a very wide bandwidth. Additionally, the intracavity loss contribution is generally smaller than with multiple-bounces GTIs. This is particularly important when it is necessary to explore the minimum achievable pulse duration and in general when the available gain bandwidth is large enough to sustain soliton pulses well below 100 fs duration. Also GTIs can be designed to provide wide-bandwidth and flat second order dispersion curves, but this is possible only when the amount of negative dispersion per bounce is very small (few tens of fs^2). For these reasons we employed GTIs only with Yb:CaF_2, which is significantly less dispersive with respect to the other oxide and tungstate crystals we tested.

Since the active media we tested differ significantly in terms of dispersive properties, nonlinear refractive index and also physical length, we also considered the option to vary the DP material with the aim of maintaining a reasonably compact resonator design. Indeed, the total resonator length influences the cavity mode radius in the active medium and consequently has an impact on the mode-matching efficiency. The available materials for prism pairs (from large to low dispersion) were: SF57, SF10, Fused Silica (FS) and CaF_2. Highly dispersive prisms allow to obtain large values of negative dispersion, easily exceeding several thousands of fs^2, with few tens of cm prisms separation. Conversely, they usually introduce higher insertion losses. Furthermore, the fine tuning of the net cavity GDD is easier with low dispersion prisms. Experimentally, we found that the optimum value of negative GDD was about -2000 fs^2 for Yb:CALGO and Yb:CALYO and about -2500 fs^2 for Yb:KLuW and Yb:SSO. In this case, SF10 proved to be the best material for DP pair. Only in case of Yb:CaF_2, given the significantly lower amount of net negative intracavity GDD required for soliton ML (about -1000 fs^2), we opted for a pair of FS prisms. In this case, we also successfully tested low (-55 fs^2 per bounce) and flat GDD GTIs in a multiple bounce configuration (see inset 4 of Fig. 1).

When we intended to explore the output wavelength tuning range in ML regime, we opted for the single DP configuration (inset 2 of Fig. 1) [16], which represents a natural choice in this case [17]. As it can be seen by the results summarized in Table 3, with Yb:CALGO, Yb:CALYO and Yb:KLuW the results obtained with the single prism setup were similar to the best results achieved with the double prism setup, further confirming the effectiveness of this solution.

For quasi-3-level materials exhibiting non-negligible reabsorption losses at the output laser wavelength, the effective distribution of gain as a function of the wavelength $g(\lambda)$ depends on the stationary population inversion, which is reached at the laser threshold. At the laser threshold, we can write:

$$g_{th}(\lambda) = 2L_g\left[N_2\sigma_e(\lambda) - N_1\sigma_a(\lambda)\right] = -\ln(R_{oc}) + \delta_c \tag{2}$$

where L_g is the active medium length, σ_e and σ_a are the wavelength dependent emission and absorption cross sections respectively, and N_2 and N_1 are the population densities of the upper and lower laser multiplets. The terms on the right-hand side of Eq. (2) can be considered wavelength-independent as long as the reflectivity/transmittivity of the optical elements in the resonator are reasonably flat across the active material gain bandwidth, as is usually the case.

By introducing the total active ions density $N_{tot} = N_1 + N_2$ (which is proportional to the

#262554 Received 5 Apr 2016; revised 11 May 2016; accepted 11 May 2016; published 20 May 2016

doping concentration) and the fraction of inverted ions $\beta = N_2/N_{tot}$, we can re-write Eq. (2) in the following way

$$\beta(\lambda) = \frac{\sigma_a(\lambda)}{\sigma_e(\lambda)+\sigma_a(\lambda)} + \frac{-\ln(R_{oc})+\delta_c}{2L_g N_{tot}(\sigma_e(\lambda)+\sigma_a(\lambda))} \tag{3}$$

where we emphasized the wavelength dependence of the β factor through the wavelength dependence of absorption and emission cross sections. Once the doping concentration, the active medium length, the reflectivity of the output coupler and the residual cavity losses are fixed, the expected laser output wavelength can be predicted by looking for the minimum of the function $\beta(\lambda)$, and the effective spectral distribution of the gain cross section will be given by

$$\sigma_{eff}(\lambda) = \beta_{min}\sigma_e(\lambda) - (1-\beta_{min})\sigma_a(\lambda) \tag{4}$$

By making use of the available spectroscopic data (absorption and emission cross sections as a function of λ) and the results of the Caird analysis, it is possible to estimate the effective β at which the laser operates and derive the effective gain cross section as a function of the wavelength. The effective gain cross section can differ significantly with respect to the emission cross section derived from spectroscopic measurement. For example, in Fig. 2 we show the effective gain spectra of Yb:CALGO calculated from our experimental conditions. For comparison we also show the spectrum corresponding to the shortest pulses obtained in the ML regime. As can be seen, a very large part of the available gain spectrum was locked, further confirming the there was no room for significant optimization of the oscillator.

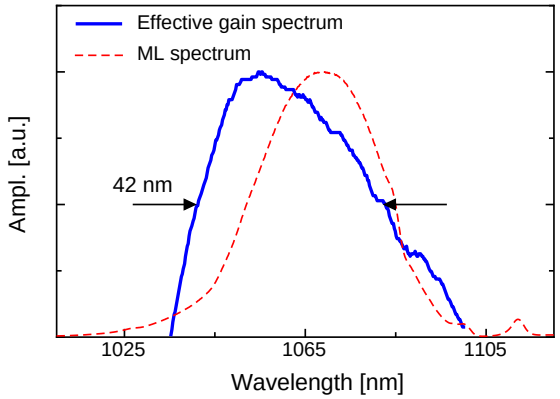

Fig. 2. Effective gain spectrum of Yb:CALGO calculated in our experimental conditions. The measured ML spectrum corresponding to the shortest pulses obtained is also shown in dashed red.

Another useful outcome of this investigation is the possibility to determine the effective ratio between the bandwidth locked in the ML regime and the available gain bandwidth offered by the active material $\xi = \Delta\lambda/\Delta\lambda_g$. This ratio, as outlined in [14], has an impact on the effective value of the intracavity pulse energy required for stabilization against Q-Switching Mode-Locking (QML) instabilities in SESAM soliton mode-locked lasers [18].

For materials exhibiting a relatively high value of the emission cross section, namely Yb:KLuW and to a lesser extent Yb:CALGO/CALYO, the ML regime was easily obtained once the cavity alignment and prism insertion was optimized. The lower saturation fluence of the active medium, as outlined in [14] is beneficial for:

#262554 Received 5 Apr 2016; revised 11 May 2016; accepted 11 May 2016; published 20 May 2016

1. reduction of the critical intracavity pulse energy required for stabilization against QML instabilities [18];

2. reduction of the energy carried by the Q-switching envelope in presence of QML instabilities, especially in the early stage of resonator alignment and optimization.

This is particularly important, since it effectively reduces the risk of SESAM damage when the laser is not yet operating in ML regime. On the other hand, materials with a relatively small emission cross section and significantly longer fluorescence lifetime (as in the case of Yb:SSO and Yb:CaF_2) require a more careful resonator design in order to overcome the intrinsically higher critical intracavity pulse energy and greater tendency to optical damage of the SESAM in presence of QML instabilities, eventually requiring a larger cavity mode area on the SESAM to avoid optical damages during the early stage of the cavity alignment (before stable ML regime is reached). According to [14, 18], the minimum intracavity pulse energy E_p required for stabilization of soliton ML regime against QML instabilities can be expressed as

$$E_p = -\frac{g\xi^2 E_g}{2} + \sqrt{\left(\frac{g\xi^2 E_g}{2}\right)^2 + E_g E_s \Delta R} \tag{5}$$

where g is the saturated gain, E_g is the saturation energy of the active medium, E_s and ΔR are the saturation energy and modulation depth of the SESAM respectively, and ξ is the fractional bandwidth of the pulse previously introduced (please note that the condition $\xi \to 0$ corresponds to the picosecond SESAM ML case).

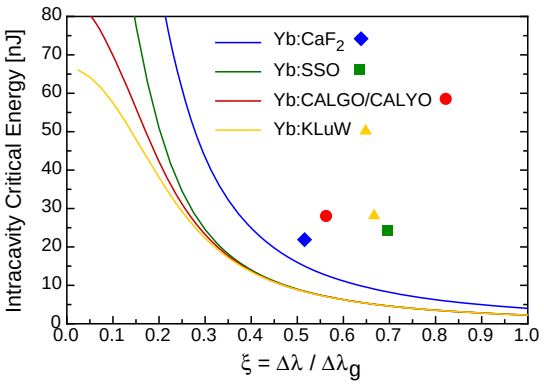

Fig. 3. Intracavity critical pulse energy calculated from our experimental conditions according to Eq. (5) (colored lines) and measured intracavity pulse energy as a function of ξ parameter at the start of the soliton ML regime (colored dots).

In Fig. 3, we present the effective intracavity critical pulse energy calculated from our experimental conditions as a function of the parameter ξ for the different active media we tested. It is worth noticing that as long as a significant fraction of the available gain bandwidth is locked (ξ >30%), the square root term of Eq. (5) in our operating conditions is dominated by the first term and the critical intracavity pulse energy mostly depends on the saturation energy and modulation depth of the SESAM [14]. This is also clear in Fig. 3, since the asymptotic value of the intracavity critical pulse energy for $\xi \to 1$ is the same for all the active materials we tested, except Yb:CaF_2. In fact, given the high energy storage capability of Yb:CaF_2, in this case, for safe operation it was necessary to increase the cavity mode area on the SESAM with

#262554 Received 5 Apr 2016; revised 11 May 2016; accepted 11 May 2016; published 20 May 2016

respect to all other materials, resulting in a correspondingly higher SESAM saturation energy E_s. In our experiments, we observed that a significant fraction of the effective available gain bandwidth ($\xi > 0.5$) was already locked as soon as sufficient negative GDD was provided and the soliton ML regime started. Afterward, when the negative GDD was progressively reduced in order to shorten the pulse, typical values of $\xi > 0.7$ were eventually achieved, resulting in a larger margin with respect to the critical intracavity pulse energy. The colored dots in Fig. 3 represent the measured intracavity pulse energy at the start of the soliton ML regime for the different materials under test.

The results obtained in the soliton ML regime at the maximum pump power, with both double dispersive prism and single dispersive prism (SP) cavity configuration are summarized in Table 3. In all the experiments, best results in terms of higher output power and shorter pulse duration were obtained for a ratio between incident and saturation fluence on the SESAM $F_{in}/F_{sat} \approx 4 \div 6$.

Table 3. Summary of the ML regime results.

	Yb:KLuW	Yb:SSO	Yb:CALGO	Yb:CALYO	Yb:CaF_2
τ_p [fs]	69	71	36	43	65
$\Delta\lambda$ [nm] (λ_c)	18 (1054)	17 (1045)	33.5 (1068)	29 (1065)	20 (1050)
$\Delta\nu\Delta\tau_p$	0.33	0.33	0.32	0.33	0.35
P_{out} [mW] (T_{oc})	45 (0.8%)	20 (0.8%)	20 (0.4%)	20 (0.4%)	35 (0.8%)
f_{rep} [MHz]	190	180	180	180	140
τ_p [fs] SP	77	109	47	45	80
$\Delta\lambda$ [nm] (λ_c) SP	16 (1058)	11 (1067)	29 (1060)	29.5 (1065)	16 (1050)
P_{out} [mW] (T_{oc}) SP	60 (0.8%)	45 (0.8%)	36 (0.4%)	30 (0.4%)	50 (0.8%)
Tuning range [nm] SP	1045–1071	1060–1070	1035–1075	1035–1075	1045–1055

Pulse durations well below 80-fs were obtained with all the materials we tested. A minimum pulse duration of 36 fs was achieved with Yb:CALGO. The pulse durations are, to the best of our knowledge, the shortest ever reported in the soliton ML regime with SESAM (for each material in this set) and only slightly longer than the latest reported record of 32 fs achieved with Kerr-lens mode-locking [19] (fastest modulation effect fully exploiting mode-locking potential). The autocorrelation trace and optical spectrum corresponding to the shortest pulses obtained by employing Yb:CALGO are shown in Fig. 4.

Exploiting the single prism setup, we could explore the maximum tuning range of the central output wavelength for all materials. Yb:CALGO and Yb:CALYO offered the best results. A continuous tuning range extending over 40 nm was possible for both materials, with a pulse duration as short as 45 fs in case of Yb:CALYO and only slightly longer (47 fs) in case of Yb:CALGO using a single FS prism and a $T = 0.4\%$ OC. In case of Yb:KLuW, due to the higher negative dispersion required we opted for a SF10 prism. The laser central output wavelength proved to be continuously tunable over more than 26 nm with a minimum 77 fs pulse duration with the $T = 0.8\%$ OC. In Fig. 5(a) we show the tuning range for Yb:CALGO and in Fig. 5(b) for Yb:KLuW.

The wavelength tuning range in the SP cavity setup was significantly narrower for Yb:SSO and Yb:CaF_2. In case of Yb:SSO, this behavior can be explained by the peculiar shape of the emission cross section which, instead of being smooth and relatively flat as in the case

#262554 Received 5 Apr 2016; revised 11 May 2016; accepted 11 May 2016; published 20 May 2016

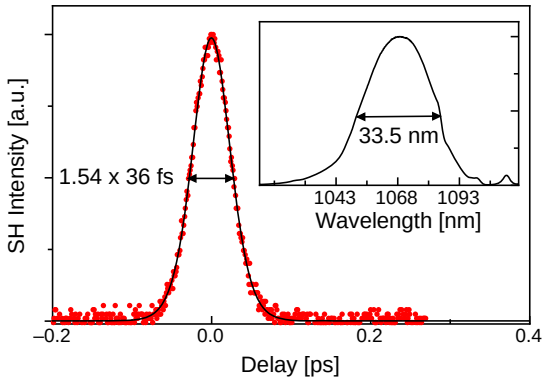

Fig. 4. Autocorrelation trace and corresponding optical spectrum (inset) of the shortest pulses obtained with Yb:CALGO.

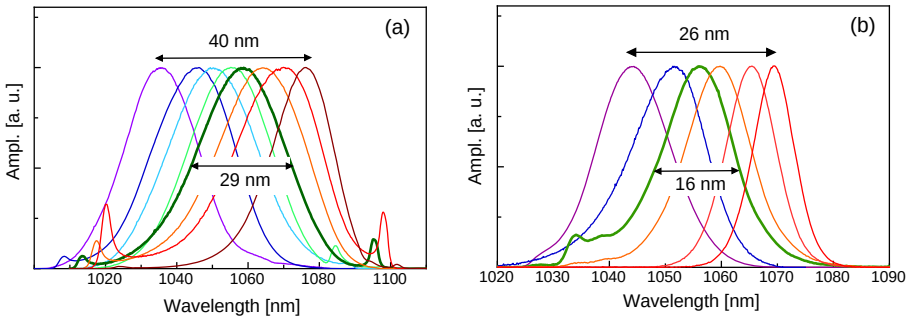

Fig. 5. Central output wavelength tuning range in single DP setup for Yb:CALGO (a) and Yb:KLuW (b).

of Yb:CALGO/CALYO, exhibits two main peaks centered at about 1036 and 1062 nm [7]. Wavelength tuning was possible only around the second peak at 1062 nm and when the center wavelength was moved towards 1050 nm, the suppression of a CW component in the spectrum centered at 1045 was not possible. In case of Yb:CaF_2, we attributed the limited central output wavelength tuning range to the relatively small margin between the actual and critical intracavity pulse energy at which the laser was operating with respect to the other materials.

3. Conclusions

In conclusion, we presented a comparative study of the performance of five different Yb-doped laser materials, all tested in a finely optimized, low-power single-mode diode pumped femtosecond oscillator. The materials we studied belong to different crystal families (tungstate, silicates, fluorides and oxides) with very large gain bandwidths and fair/good thermo-mechanical properties that are very attractive for the next generation of industrial ultrafast solid-state lasers and amplifiers. Exploiting the advantages of single-mode diode pumping, through a careful optimization of the femtosecond resonator design and owing to the improvements of the SESAM technology, we were able to obtain with all materials, to the best of our knowledge, the shortest pulse reported in literature in the SESAM soliton ML regime (record of 36 fs with Yb:CALGO). We investigated the ultimate limits and potential of these materials by analyzing the effective gain bandwidth offered by the quasi-three level active media in our experimental conditions.

#262554 Received 5 Apr 2016; revised 11 May 2016; accepted 11 May 2016; published 20 May 2016

Due to the presence of reabsorption losses, the fraction of inverted ions $\beta = N_2/N_{tot}$ at which the laser operates, strongly affects both the shape and width of the effective gain spectrum of the quasi-three level laser. The materials offering the widest and smoothest effective gain bandwidth were Yb:CALGO and Yb:CALYO and they outperformed the others in terms of shortest pulse duration in the soliton ML regime and wavelength tuning range. Yb:CaF_2 required a more careful resonator design, mainly because of the unfavorable combination of a low value of emission cross section and a long fluorescence lifetime that favors the optical damage of the SESAM in presence of QML instabilities. Despite offering only slightly narrower effective gain bandwidth with respect to CALGO/CALYO, the minimum pulse duration obtained with Yb:CaF_2 was significantly longer and similar to the more straightforward and efficient Yb:KLuW laser. The presence of multiple peaks in the effective gain spectrum was the main limiting factor to the ultimate pulse shortening and tuning range of Yb:SSO, which is nevertheless a very attractive material in particular for high energy femtosecond pulse amplification.

#262554 Received 5 Apr 2016; revised 11 May 2016; accepted 11 May 2016; published 20 May 2016